

Zinc Thiolate Complexes $[\text{ZnL}_n(\text{SR})]^+$ with Azamacrocyclic Ligands, Part II: Mechanism of the Reaction with CS_2 ^[‡]

Johannes Notni,^[a] Stephan Schenk,^[a] Arne Roth,^[b] Winfried Plass,^[b] Helmar Görls,^[c]
 Ute Uhlemann,^[d] Angela Walter,^[d] Michael Schmitt,^[d] Jürgen Popp,^[d]
 Susana Chatzipapadopoulou,^[d] Thomas Emmeler,^[e] Hergen Breitzke,^[d] Jörg Leppert,^[f]
 Gerd Buntkowsky,^[d] Kristian Kempe,^[a] and Ernst Anders*^[a]

Keywords: Zinc / Macrocyclic ligands / Enzyme models / Heterocumulenes / Density functional calculations

The thiolate complexes $[\text{Zn}(\text{[15]aneN}_4)(\text{S}-\text{CH}_2-\text{C}_6\text{H}_5)]\text{ClO}_4$ (**1**) ($[\text{15]aneN}_4 = 1,4,8,12\text{-tetraazacyclopentadecane}$) and $[\text{Zn}(i\text{-[14]aneN}_4)(\text{S}-\text{CH}_2-\text{C}_6\text{H}_5)]\text{ClO}_4$ (**2**) ($i\text{-[14]aneN}_4 = 1,4,7,11\text{-tetraazacyclotetradecane}$) have been reacted with carbon disulfide. The trithiocarbonate complexes $[\text{Zn}(\text{[15]aneN}_4)\{\text{S}-\text{C}(\text{S})-\text{S}-\text{CH}_2-\text{C}_6\text{H}_5\}]\text{ClO}_4$ (**1a**, monoclinic, space group $P2_1/n$, $Z = 8$, $a = 13.2338(1) \text{ \AA}$, $b = 12.9251(2) \text{ \AA}$, $c = 30.1669(4) \text{ \AA}$, $\beta = 101.463(1)^\circ$, $V = 5057.1(1) \text{ \AA}^3$) and $[\text{Zn}(i\text{-[14]aneN}_4)\{\text{S}-\text{C}(\text{S})-\text{S}-\text{CH}_2-\text{C}_6\text{H}_5\}]\text{ClO}_4$ (**2a**, orthorhombic, space group $P2_12_12_1$, $Z = 8$, $a = 9.9936(1) \text{ \AA}$, $b = 22.1261(4) \text{ \AA}$, $c = 22.3192(4) \text{ \AA}$, $V = 4935.2(1) \text{ \AA}^3$) were obtained. The reaction of **1** with CS_2 is second order with a rate constant of $k = (57.6 \pm 2.4) \times 10^{-3} \text{ M}^{-1}\text{s}^{-1}$ at 25°C . The experimentally deter-

mined Eyring activation barrier is $\Delta H_{\text{exp}}^\ddagger = 65.3 \pm 0.7 \text{ kJ}\cdot\text{mol}^{-1}$ ($\Delta S_{\text{exp}}^\ddagger = -49.9 \pm 2.5 \text{ J}\cdot\text{mol}^{-1}\cdot\text{K}^{-1}$) and a free energy of activation of $\Delta G^\ddagger = 80.2 \pm 1.5 \text{ kJ}\cdot\text{mol}^{-1}$ at 25°C . To discriminate between an associative and a dissociative mechanism the barriers for both processes were calculated using density functional theory at the C-PCM(B98/G3MP2Large)//B3LYP/6-311+G(d) level. The associative mechanism is clearly favored with a difference in free energies of activation of $\delta\Delta G^\ddagger \approx 80 \text{ kJ}\cdot\text{mol}^{-1}$. Its calculated barrier $\Delta G_{\text{theor}}^\ddagger = 114.3 \text{ kJ}\cdot\text{mol}^{-1}$ is in reasonable agreement with the experimental value.

(© Wiley-VCH Verlag GmbH & Co. KGaA, 69451 Weinheim, Germany, 2006)

Introduction

Carbonic anhydrase (CA) is a ubiquitous zinc enzyme that accelerates the reversible hydration of CO_2 by a factor of up to 10^7 when compared with the uncatalyzed reaction.^[2–4] This enzymatic process is very important in all living organisms for the exchange of CO_2 with the atmosphere. (Detailed references to the numerous studies concerning the catalytic mechanism are given elsewhere.^[2,5]) The rate-determining step of the reaction is the nucleophilic attack of a zinc-bound hydroxide ligand on carbon dioxide.

From quantum mechanical calculations it has been concluded that the reaction proceeds via a four-center transition structure (see Scheme 1).^[6,7]

Recent studies of Kesselmeier et al. have shown that CA is also implicated in the fixation of COS, a sulfur-containing heterocumulene that occurs as a trace gas in the atmosphere.^[8] This process is performed by many organisms, such as higher plants,^[9] algae,^[10] lichens,^[11] and even by components of the soil.^[12] This interconversion has been reproduced experimentally by reacting an established CA model, $[\text{Tp}^{\text{Ph,Me}}\text{ZnOH}]$, with COS.^[13] In the course of the reaction, CO_2 is released and the sulfur-analog complex $\text{Tp}^{\text{Ph,Me}}\text{ZnSH}$ is obtained. In addition, this complex is also formed by reacting $\text{Tp}^{\text{Ph,Me}}\text{ZnOH}$ with CS_2 . In this case, COS is produced instead of CO_2 , which in turn is capable of reacting with the zinc hydroxide complex to yield CO_2 . This type of reaction, the fixation of sulfur-containing heterocumulenes by CA model compounds, has also been studied by us using computational methods.^[5,14] In analogy to the fixation of CO_2 , it has been found for all the studied systems that the insertion of the heterocumulene into the Zn–O bond via a four-center transition structure is the rate-determining step of the reaction.^[5,6,14]

These studies show that the reaction of natural carbonic anhydrase is likely to result in the formation of a sulfur-analog enzyme with a hydrosulfide instead of a hydroxide

[‡] For further reference see: Zinc Thiolate Complexes $[\text{ZnL}_n(\text{SR})]^+$ with Azamacrocyclic Ligands, Part I: Synthesis and Structural Properties^[1]

[a] FSU Jena, Institut für Organische Chemie und Makromolekulare Chemie,
 Humboldtstr. 10, 07743 Jena, Germany

E-mail: ernst.anders@uni-jena.de

[b] FSU Jena, Institut für Anorganische und Analytische Chemie, Carl-Zeiss-Promenade 10, 07745 Jena, Germany

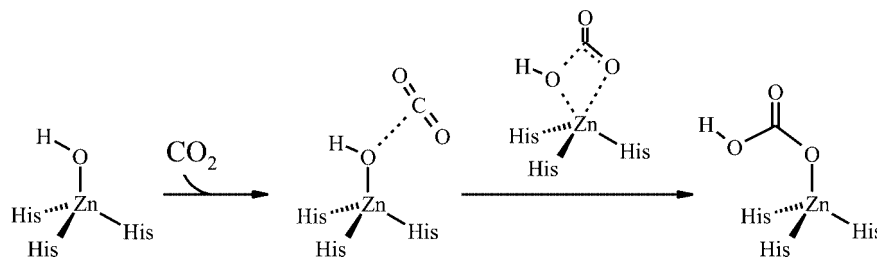
[c] FSU Jena, Institut für Anorganische und Analytische Chemie, Lessingstr. 8, 07743 Jena, Germany

[d] FSU Jena, Institut für Physikalische Chemie, Helmholtzweg 4, 07743 Jena

[e] FU Berlin, Institut für Chemie und Biochemie, Takustr. 3, 14195 Berlin

[f] Leibniz Institut für Altersforschung, Beutenbergstr. 11, 07745 Jena

Supporting information for this article is available on the WWW under <http://www.eurjic.org> or from the author.



Scheme 1. Insertion of carbon dioxide into the Zn-S bond of CA.

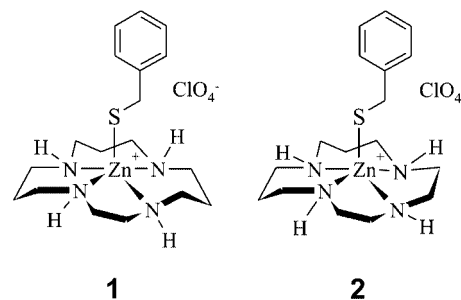
ligand. Since this reaction is exothermic, natural CA would become inactivated in this ‘sulfurated state’.^[5] Kesselmeier et al. have pointed out, though, that in the case of lichens, atmospheric sulfur compounds are the only available source of sulfur.^[11] Apparently, the fixation of sulfur-containing compounds by CA is not a side reaction but rather essential for some organisms. This gives rise to the question of how CA can dispose of the sulfur in order to be reactivated. In a preceding theoretical study of a CA model system, a nucleophilic reaction of the Zn-SH moiety with CO₂ has been proposed for regeneration of the active catalyst.^[5] However, until now this theory has not been supported by any experimental investigations.

In this work, we report on a reaction of the CS₂ with a zinc thiolate complex. We are fully aware that this may seem to be a large stretch of the subject. Nevertheless, the results are of value for the understanding of the reaction principles of a zinc-bound sulfur nucleophile with heterocumulenes in general. It is worth noting that a similar reaction has not previously been reported in the literature; even the available structural models for the sulfur-analog CA, e.g. Tp^{Ph,Me}ZnSH,^[15] do not react with heterocumulenes. In the past, numerous computational studies have examined the fixation of heterocumulenes by zinc hydroxide complexes, but only one addresses zinc hydrosulfides and the mechanism of their heterocumulene reactions.^[5] The results presented in this work are the first steps in elucidating the mode of heterocumulene fixation by sulfur-analog CA models. Investigations concerning the reactions of COS and CO₂ will be published soon.

Results

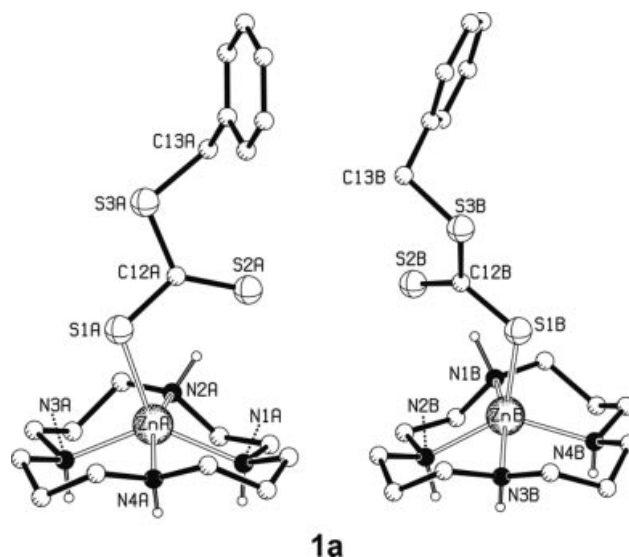
Heterocumulene Insertions

The starting materials, thiolate complexes **1** and **2** (see Scheme 2), are examples of a series of 24 novel zinc thiolate complexes.^[1] The progress of the CS₂ insertion reaction can easily be monitored by the appearance of a yellow color from the formation of the trithiocarbonates. When reacting the neat substances with CS₂, only a very slow reaction was observed. This is not surprising, since the thiolates are virtually insoluble in CS₂. The reaction is obviously not possible while the complex cations are fixed in the crystal lattice. In contrast to this, the reaction proceeds quite fast when the starting materials are dissolved.

Scheme 2. Thiolate complexes **1** and **2**.

Structures

Compounds **1a** (Figure 1) and **2a** (Figure 2) precipitated from concentrated dichloromethane solutions upon addition of a large excess of CS₂. Yellow crystals were obtained that were subjected to an X-ray crystallographic structure determination. The configuration of the four N atoms in the trithiocarbonates is the same as that found for the corresponding thiolates.^[1] One of the N-bound hydrogens is found on the opposite side of the ligand and three are located on the opposite side [the so-called (+ - - -) configuration^[16,17]]. For both compounds, the crystal lattices comprise two independent molecules with differences in conformation and bond lengths. In the case of **1a**, these

Figure 1. Molecular structures of the trithiocarbonate complex cation of **1a**.

two molecules are enantiomers because of the configuration of the nitrogen donors, which does not match the symmetry of the ligand, as was found for **2a**. However, the structural parameters of all trithiocarbonate moieties show very little variation and the Zn–S distances of both **1a** and **2a** are almost identical (Table 1).

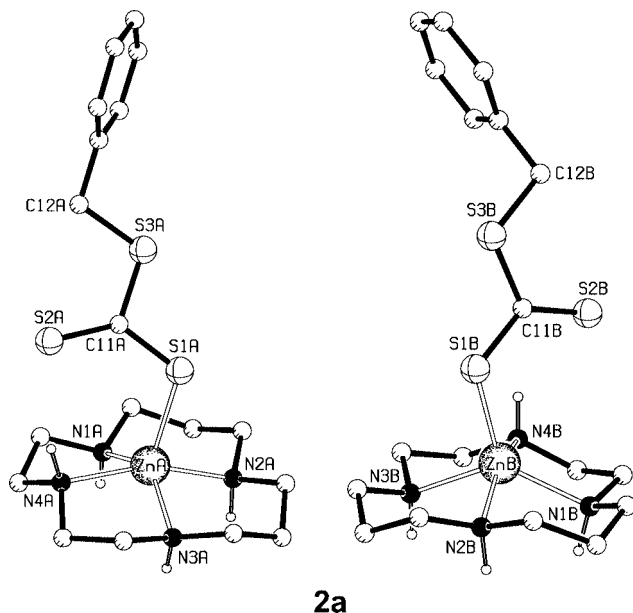


Figure 2. Molecular structures of the trithiocarbonate complex cation of **2a**.

Table 1. Selected bond lengths [Å] and angles [°] for **1a** and **2a** (atom numbers of **2a** are given in parentheses where they are different from **1a**).

Value	1a (A)	1a (B)	2a (A)	2a (B)
Zn–S1	2.373(1)	2.363(1)	2.373(1)	2.353(1)
Zn–N1	2.153(4)	2.187(4)	2.101(4)	2.110(4)
Zn–N2	2.188(3)	2.117(4)	2.144(3)	2.176(4)
Zn–N3	2.117(3)	2.209(3)	2.106(4)	2.149(4)
Zn–N4	2.169(3)	2.110(3)	2.149(4)	2.185(4)
C12(C11)–S1	1.723(3)	1.720(4)	1.722(4)	1.708(4)
C12(C11)–S2	1.639(4)	1.640(4)	1.658(4)	1.652(5)
C12(C11)–S3	1.750(3)	1.756(3)	1.739(4)	1.755(5)
S3–C13(C12)	1.806(4)	1.816(4)	1.813(5)	1.823(6)
Zn–S1–C12(C11)	107.3(1)	108.6(1)	112.5(2)	109.9(2)
S1–C12(C11)–S2	126.8(2)	128.0(2)	130.3(3)	128.1(3)
S1–C12(C11)–S3	108.4(2)	108.2(2)	108.2(2)	108.9(3)
S2–C12(C11)–S2	124.8(2)	134.8(2)	121.4(2)	123.0(3)
C12(C13)–S3–C13(C12)	105.6(2)	105.7(2)	105.3(2)	106.1(3)

NMR Spectra

For the NMR spectroscopic investigations, chloroform solutions of **1** and **2** containing an equimolar amount and a 10-fold excess of CS₂ were analyzed. In these solutions, complexes **1a** and **2a** exist in a dynamic equilibrium with **1** and **2**, respectively (see Scheme 4). This causes all carbon atoms, particularly the trithiocarbonate carbons, to exhibit an increased line width in the ¹³C spectra. Thus, their detection requires a large number of scans (>10.000) in order to reduce the signal-to-noise ratio.

Table 2 shows that upon addition of a 10-fold molar excess of CS₂ compound **1** is converted nearly completely to the trithiocarbonate **1a**, whereas the turnover is only two thirds for **2a** under the same conditions. This renders the reaction of **1** to **1a** suitable for the investigation of subsequent reactions and for determination of the thermal parameters of the insertion. Furthermore, it is worth noting that small changes of the macrocyclic ligand can have a dramatic effect on the reactivity of the thiolate, even though the structural parameters of the substrates and the products are nearly identical.

Table 2. Turnover of thiolates to trithiocarbonates in chloroform solutions containing different amounts of CS₂ (derived from ¹H NMR spectroscopic data).

Mol. equiv. of CS ₂	1a [%]	2a [%]
1	50	19
10	>98	67

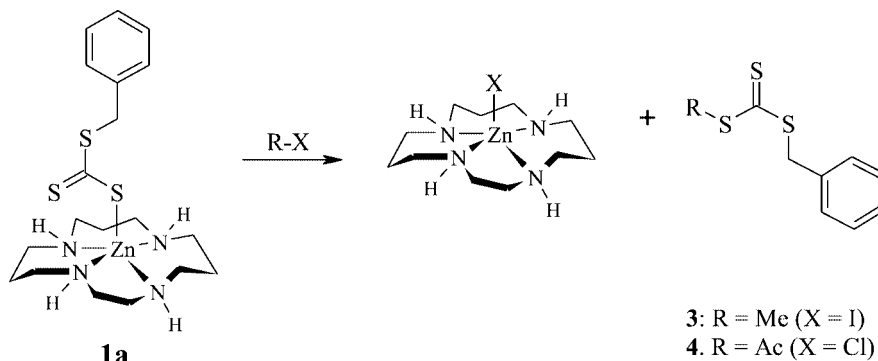
The ¹³C NMR spectrum of **1a** shows 12 methylene signals. This indicates that the molecule has an asymmetric structure in a chloroform solution. It is most probable that the (+ – –)–configuration is adopted, analogous with the solid-state structure. In contrast to the thiolate complex **1**,^[1] the NMR spectra of **1a** do not provide any evidence for the presence of a second configurational isomer. As mentioned above, the zinc(II) ion of **1a** is chiral in nature due to the asymmetric configuration of the macrocyclic ligand. Thus, the benzyl protons of **1a** are in a diastereotopic environment. Nevertheless, the increased multiplicity of the corresponding NMR signals found for **1**^[1] was not observed in the ¹H NMR spectrum of **1a**. This is a result of the spacer function of the trithiocarbonate moiety. The benzyl protons of **1a** are located at a much larger distance from the zinc atom than in complex **1**. The influence of the center of chirality is thus reduced to a minimum.

Solid-State NMR Spectroscopy

While the thiolate complexes **1** and **2** do not have any spectral intensity in the range 230–240 ppm, the ¹³C NMR spectra of the insertion products show strong signals in this spectral region. These lines show the formation of a thiocarbonyl group and thus corroborate the proposed structure of the trithiocarbonate moiety. Interestingly, both the thiocarbonyl line of **1a** and the line of the quaternary aromatic carbon C14 exhibit a splitting into an asymmetric doublet. These splittings reflect the conformational polymorphism of **1a**, which obviously is not as pronounced in **2a**. A splitting of the corresponding lines could not be observed in this case. (For graphical representations of all spectra and peak assignments see the Supporting Information.)

Raman Spectroscopy

Complexes **1** and **1a** have also been investigated using Raman spectroscopy. Two strong signals at 507 and 1032 cm⁻¹ appear in the spectra of the reaction product **1a**. These are because of the symmetric (SCS) and the (C=S)



Scheme 3. Reaction of the trithiocarbonate complex **1a** with electrophiles (only cations shown).

vibration, respectively, which correspond to the trithiocarbonate moiety of **1a**. At the same time, a signal at 1223 cm^{-1} decreases in intensity. Raman monitoring of the reaction has shown that the formation of **1a** occurs in a clean reaction. Currently, we have no evidence for the formation of any intermediates or side products. (For a graphical representation of the spectra and a more detailed discussion see Supporting Information.)

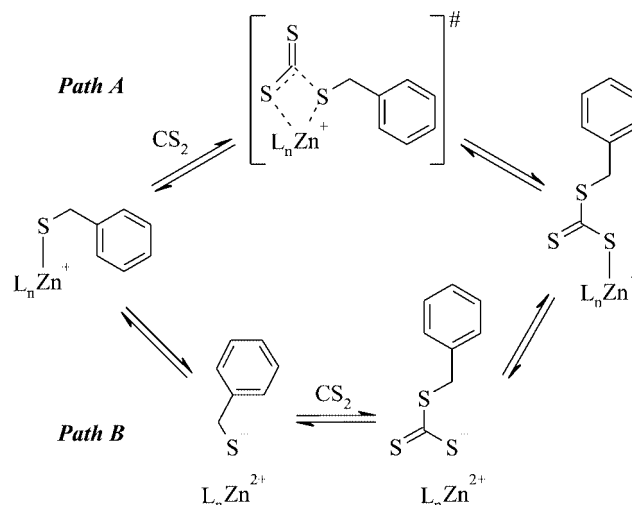
Reactions of Complex **1a**

Similar to the thiolates, the trithiocarbonate complexes possess nucleophilic properties, as was found when reacting compound **1a** with electrophiles (see Scheme 3). Methyl iodide was added to a concentrated solution of **1** with a 10-fold excess of CS_2 . As mentioned above, under these conditions the equilibrium is almost completely shifted to the insertion product **1a**. However, the reaction product of **1** with methyl iodide, which is benzyl methyl sulfide, was isolated in approx. 20% yield. Obviously, the thiolate **1** reacts several times faster than the trithiocarbonate **1a**, most likely because of the higher nucleophilicity of the thiolate sulfur in **1**. The quenching reaction with acetyl chloride results in the formation of the corresponding acetyl-substituted benzyltrithiocarbonate. The products were isolated and identified by their NMR spectra, which were known from authentic samples prepared for this purpose (see Exp. Sect.).

Mechanism of CS_2 Insertion

The possible reaction mechanisms for the insertion of CS_2 into the Zn-S bond are outlined in Scheme 4. An attack of the zinc-bound thiolate on the carbon disulfide should result in clean second-order kinetic behavior of the reaction (path A). We assume that this is the preferred mechanism in a nonpolar solvent. An attack of the free thiolate (path B) should be much faster than the preliminary dissociation of the complex and result in clean first-order kinetics. Nevertheless, one could possibly observe second-order kinetics because of the perturbation effects or in the case where the dissociation step is unexpectedly not much slower than the CS_2 reaction. Thus, both mechanisms cannot be distinguished simply by comparing the order of their reaction kinetics. It is highly improbable, though, that

the actual rate constants and activation barriers of both reaction modes are identical. Hence, we determined the activation barrier of this reaction and compared it with the calculated value for both of the possible pathways.



Scheme 4. Possible mechanisms for the formation of the trithiocarbonate complexes **1a** and **2a**.

Kinetic Study

Since the insertion product **1a** absorbs at 434 nm the reaction progress could be monitored using electronic spectroscopy. At room temperature, the reaction proceeds on a time scale of minutes. Thus it was convenient to measure the rate constants at temperatures between 10 and 35 °C.

Because the reaction is an equilibrium reaction, the obtained data are a superposition of forward and backward reactions. In order to determine only the kinetic parameters of the insertion reaction, the perturbation effect of the back reaction must be eliminated. This was achieved by reacting **1** with CS_2 under pseudo first-order conditions. Only the data collected immediately after the start of the reaction were employed for the calculation of the rate constants.

A solution of **1** (0.05 M) was treated with a 20-fold excess of carbon disulfide. Under these conditions, the equilibrium is virtually completely shifted to the side of the insertion product. This was verified by NMR spectroscopy. The loga-

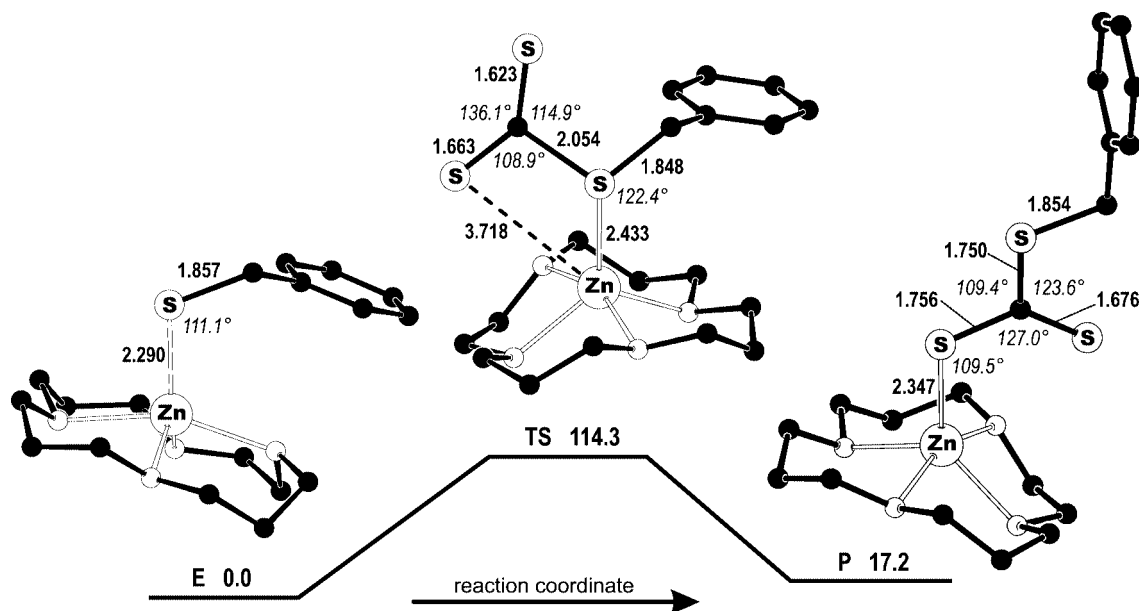


Figure 3. Structures and energy profile of the fixation of CS_2 by **1**, calculated at the C-PCM(B98/G3MP2Large)//B3LYP/6-311+G(d) level of theory. ΔG values are given in $\text{kJ}\cdot\text{mol}^{-1}$.

rithmic plots employed for the calculation of the rate constants show only a very small variation from linearity with standard deviations of less than 1%. This emphasizes the clean pseudo first-order kinetic behavior of the observed reaction and proves that the perturbation effect of the back reaction is insignificant. Thus, the obtained kinetic and thermal parameters reliably represent the second-order insertion reaction. Analysis of a data set of 21 rate constants according to the Eyring theory resulted in $\Delta H^\ddagger = 65.3 \pm 0.7 \text{ kJ}\cdot\text{mol}^{-1}$ and $\Delta S^\ddagger = -49.9 \pm 2.5 \text{ J}\cdot\text{mol}^{-1}\cdot\text{K}^{-1}$. The resulting free energy of activation at 25 °C is $\Delta G^\ddagger = 80.2 \pm 1.5 \text{ kJ}\cdot\text{mol}^{-1}$.

Quantum Mechanical Calculations

The geometries of the starting material (**E**), the transition structure (**TS**), and the product (**P**) of the associative mechanism were optimized at the B3LYP/6-311+G(d) level of theory (Figure 3). For both **E** and **P** the X-ray structures of **1** and **1a**, respectively, served as starting points. The effect of the solvent chloroform on the reaction has been incorporated through the C-PCM model by B98/G3MP2Large single point calculations using the previously optimized B3LYP gas phase geometries. (For more detailed information see Computational Details.)

For the associative mechanism, the free energy of activation was calculated to be $\Delta G^\ddagger = 114.3 \text{ kJ}\cdot\text{mol}^{-1}$. For comparison with the experimental results, the enthalpy of activation was computed to be $\Delta H^\ddagger = 60.7 \text{ kJ}\cdot\text{mol}^{-1}$. The overall reaction is slightly endergonic ($\Delta_R G = 17.2 \text{ kJ}\cdot\text{mol}^{-1}$).

For the dissociative mechanism a lower limit for the activation energy was estimated by calculating the energy required for the dissociation of **1** according to Equation (1) at the same level of theory. The initial dissociation of **E**

requires $\Delta G = 191.8 \text{ kJ}\cdot\text{mol}^{-1}$ and the barrier is thus quite substantial. Upon reaction with CS_2 the energy decreases slightly to $\Delta G = 165.4 \text{ kJ}\cdot\text{mol}^{-1}$.



Discussion

The main issue we want to address in this work is the question of whether insertion of CS_2 proceeds via an associative mechanism or via a dissociative mechanism involving free thiolate. Preceding work has shown that the insertion of heterocumulenes into Zn-X ($\text{X} = \text{O}, \text{S}$) bonds usually involves a four-center transition structure.^[5–7,13,14,18] For this type of reaction, this structure generally represents the rate-determining step. For the reaction we investigated, we thus proposed a mechanism that features a similar four-center transition structure, **TS**. In addition, it is highly improbable that the missing reaction step, the rearrangement (i.e. bond rotation) that leads to the reaction product **P**, involves an intermediate with a higher energy than the insertion step. No such example has been reported in the literature. Hence, we conclude that the free energy of the transition structure **TS** constitutes the actual reaction barrier and is thus comparable to the experimental value. Therefore, the different mechanisms can be distinguished by directly comparing the barriers and by comparison with the experimentally determined value.

From the calculations it is evident that the associative mechanism is favored by approximately $80 \text{ kJ}\cdot\text{mol}^{-1}$ ($\Delta G^\ddagger = 114.3 \text{ kJ}\cdot\text{mol}^{-1}$ for path A compared with $\Delta G^\ddagger > 190 \text{ kJ}\cdot\text{mol}^{-1}$ for path B). Obviously, the entropy gain accompanying dissociation is not large enough to counterbal-

ance the unfavorable reaction enthalpy. Furthermore, the calculated barrier of path A ($\Delta G^\ddagger = 114.3 \text{ kJ}\cdot\text{mol}^{-1}$) is in reasonable agreement, although somewhat larger, with the experimental value ($\Delta G^\ddagger = 80.2 \text{ kJ}\cdot\text{mol}^{-1}$).

In addition, we would like to emphasize the good agreement of the values for the enthalpy of activation (ΔH^\ddagger) obtained experimentally and theoretically. The correlation ($\Delta H_{\text{exp}}^\ddagger = 65.3 \pm 0.7 \text{ kJ}\cdot\text{mol}^{-1}$ versus $\Delta H_{\text{theor}}^\ddagger = 60.7 \text{ kJ}\cdot\text{mol}^{-1}$) is striking, with a difference of only $5 \text{ kJ}\cdot\text{mol}^{-1}$. Naturally, a very good agreement is therefore also obtained for the activation energy (E_a) according to the Arrhenius equation. The experimentally determined value is $E_{a(\text{exp})} = 67.8 \pm 0.8 \text{ kJ}\cdot\text{mol}^{-1}$ compared to a computed value of $E_{a(\text{theor})} = 63.2 \text{ kJ}\cdot\text{mol}^{-1}$. (Admittedly, it is also possible that we benefit from some kind of fortuitous error cancellation here. However, with respect to the error margins of the computation this is not of significance concerning the overall conclusions of this work.)

The data presented above provides strong evidence that the insertion of CS_2 proceeds via an associative mechanism and that a dissociative mechanism is very unlikely under the chosen experimental conditions. Moreover, the applied technique of using gas-phase geometries and deriving energies from single-point C-PCM calculations can only yield results of restricted accuracy. We thus assume that the deviations of the calculated energies from experimental data are mainly caused by these deficiencies in the treatment of solvent effects.

Conclusions

The chemistry of the $L_n\text{Zn}-\text{XR}$ motif ($X = \text{O}, \text{S}; R = \text{H}, \text{alkyl}, \text{aryl}; L_n$: 3 or 4 nitrogen donors) is highly relevant to biosystems. The heterocumulene reactions of these systems follow two basic principles: First, the nucleophilic attack of the zinc-bound heteroatom is facilitated by the polarizing effect of the $\text{Zn}-\text{X}$ linkage on the heterocumulene. Second, the zinc(II) ion is able to accept a variety of coordination numbers and geometries and thus even severely distorted transition structures are possible. For these reasons, nucleophilic anions in zinc complexes can attack the heterocumulene in a zinc-bound state rather than acting as free (dissociated) anions. We would like to point out that in several studies an associative (zinc-bound) mechanism was invariably found for heterocumulene reactions of widely different examples of $L_n\text{Zn}-\text{XR}$ complexes: for sterically unsaturated species such as $[(\text{py})_n\text{Zn}-\text{OH}]^+$ and $[(\text{im})_n\text{Zn}-\text{OH}]^+$ ($n = 1-3$) with CO_2 ,^[18] for several species resembling the 'classic' CA motif $[\text{N}_3\text{Zn}-\text{OH}]^+$ with CO_2 ,^[6,7,19] COS ,^[5] and CS_2 ,^[13,14] and for sterically demanding zinc thiolates with CS_2 (this work). Thus, we conclude that the principle of heterocumulene fixation involving a four-center transition structure is generally applicable and largely independent of the nature of the heterocumulene and the nucleophilic ligand (XR).

Currently, these investigations are being extended to other heterocumulene substrates, namely COS and CO_2 . In

this case, the elucidation of molecular structures of the products is much more difficult due to the fact that it is apparently not possible to obtain a standard NMR spectroscopic or an X-ray structural analysis. Thus, additional spectroscopic investigations are required, namely solid-state NMR and Raman spectroscopy. In the present work, these methods were applied for calibration purposes and appear to be of great value for determining structural details. A report on this continued study will be available soon.

Experimental Section

General: All reagents used were of analytical purity. NMR spectra were recorded using a Bruker AC 250 or AC 400 spectrometer, respectively, at a temperature of 30°C . IR data was collected from the neat substances using a Nicolet Avatar 320 FT-IR spectrometer. Elemental analysis was performed using a Heraeus Vario EL III system. Melting points were determined with a Büchi Melting Point B545 apparatus and are uncorrected. Raman measurements were performed on a LabRam HR inverse spectrometer (Jobin Yvon) with an excitation wavelength of 532 nm (Nd:YAG laser). A $100\times$ objective was used to focus the laser beam on the sample. With a 300 lines/mm grating and a CCD detector, a spectral resolution of 5 cm^{-1} was reached. The accumulation time was between 30 and 120 s.

[Zn([15]aneN₄){S-C(S)-SCH₂C₆H₅}ClO₄ (1a): Complex **1** (250 mg) was dissolved in a minimal amount (ca. 0.5 mL) of dichloromethane. CS_2 (2 mL) was then added to this solution. The mixture immediately turned yellow. After a short time, yellow crystals formed, which were separated and washed with a small amount of CS_2 . Yield: 85%. M.p. = $112-113^\circ\text{C}$. $\text{C}_{19}\text{H}_{33}\text{N}_4\text{S}_3\text{ClO}_4\text{Zn}$ (578.49): calcd. C 39.45, H 5.75, Cl 6.13, N 9.68, S 16.63; found C 39.27, H 5.92, Cl 6.27, N 9.69, S 16.63. IR: $\tilde{\nu} = 3252$ (m), 2925 (m), 2864 (m), 1071 (vs), 1024 (vs), 821 (s), 706 (s), 620 (s) cm^{-1} . NMR: 25 mg of **1** in 0.4 mL chloroform with a 10-fold molar excess of CS_2 , contains virtually exclusively complex **1a** and only traces of **1**. ^1H NMR (400 MHz, CDCl_3): $\delta = 1.75-1.95$ (range of multiplets, 7 H), 2.63-3.83 (range of multiplets, 21 H), 4.44 (s, 2 H, Ar- CH_2), 7.21-7.30 (multiplet, 5 H, Ar- H) ppm. ^{13}C NMR (100 MHz, CDCl_3 , 13911 scans): $\delta = 24.8, 27.9, 28.1, 46.2, 47.1, 48.3, 49.8, 51.4, 52.3, 52.4, 53.8, 54.0, 127.3, 128.5, 129.2, 135.8, 239.0$ ppm.

[Zn(*i*-[14]aneN₄){S-C(S)-SCH₂C₆H₅}ClO₄ (2a): The preparation was carried out similarly to that for **1a**. Yield: 81%. No melting point detectable; decomposition at $115-120^\circ\text{C}$ yields the thiolate complex **2**. $\text{C}_{18}\text{H}_{31}\text{N}_4\text{S}_3\text{ClO}_4\text{Zn}$ (564.47): calcd. C 38.30, H 5.54, Cl 6.28, N 9.96, S 17.04; found C 38.19, H 5.43, Cl 6.27, N 9.96, S 16.89. IR: $\tilde{\nu} = 3260$ (m), 3165 (w), 2919 (m), 2866 (m), 1080 (s), 1076 (vs), 1033 (vs), 975 (s), 930 (s), 812 (s), 716 (m), 621 (vs) cm^{-1} . NMR: 25 mg of **2** in 0.4 mL chloroform with a 10-fold molar excess of CS_2 , contains approx. 67% of complex **2a** and 33% of **2**. ^1H NMR (400 MHz, CDCl_3): $\delta = 1.8-3.4$ (range of multiplets), 4.48 (s, Ar- CH_2), 7.25-7.36 (multiplet, Ar- H) ppm. ^{13}C NMR (100 MHz, CDCl_3): $\delta = 27.9, 45.8, 47.7, 49.1, 50.2, 51.9, 128.0, 128.5, 129.1, 135.8, 238.9$ ppm.

Crystal Structure Determination

The intensity data was collected on a Nonius Kappa CCD diffractometer, using graphite-monochromated $\text{Mo-K}\alpha$ radiation. Data was corrected for Lorentz and polarization effects, but not for absorption effects.^[20,21] The structures were solved by direct methods (SHELXS^[22]) and refined by full-matrix least-squares

techniques against F_o^2 (SHELXL-97^[23]). The hydrogen atoms of the amine groups were located by difference Fourier synthesis and refined isotropically. All other hydrogen atoms were included at calculated positions with fixed thermal parameters. All non-hydrogen atoms were refined anisotropically.^[23] XP (SIEMENS Analytical X-ray Instruments, Inc.) was used for structure representations. The drawings in the paper were generated using the program PLATON.^[24]

Crystal Data for 1a:^[25] $\text{C}_{19}\text{H}_{33}\text{N}_4\text{S}_3\text{Zn}\cdot\text{ClO}_4$, $M_r = 578.49 \text{ g}\cdot\text{mol}^{-1}$, yellow prism, size $0.03 \times 0.03 \times 0.02 \text{ mm}$, monoclinic, space group $P2_1/n$, $a = 13.2338(1)$, $b = 12.9251(2)$, $c = 30.1669(4) \text{ \AA}$, $\beta = 101.463(1)^\circ$, $V = 5057.1(1) \text{ \AA}^3$, $T = -90^\circ \text{C}$, $Z = 8$, $\rho(\text{calcd.}) = 1.520 \text{ g}\cdot\text{cm}^{-3}$, $\mu(\text{Mo-K}\alpha) = 13.58 \text{ cm}^{-1}$, $F(000) = 2416$, 20403 reflections in $h(-17/17)$, $k(-16/15)$, $l(-39/39)$, measured in the range $1.84^\circ \leq \theta \leq 27.49^\circ$, completeness $\theta_{\text{max}} = 98.5\%$, 11426 independent reflections, $R_{\text{int}} = 0.049$, 6885 reflections with $F_o > 4(F_\sigma)$, 608 parameters, $R1_{\text{obs}} = 0.049$, $wR2_{\text{obs}} = 0.103$, $R1_{\text{all}} = 0.1065$, $wR2_{\text{all}} = 0.119$, GOOF = 1.014, largest difference peak and hole: $0.676/-0.583 \text{ e}\cdot\text{\AA}^{-3}$.

Crystal Data for 2a:^[25] $\text{C}_{18}\text{H}_{31}\text{N}_4\text{S}_3\text{Zn}\cdot\text{ClO}_4$, $M_r = 564.47 \text{ g}\cdot\text{mol}^{-1}$, yellow prism, size $0.06 \times 0.05 \times 0.05 \text{ mm}^3$, orthorhombic, space group $P2_12_12_1$, $a = 9.9936(1)$, $b = 22.1261(4)$, $c = 22.3192(4) \text{ \AA}$, $V = 4935.2(1) \text{ \AA}^3$, $T = -90^\circ \text{C}$, $Z = 8$, $\rho(\text{calcd.}) = 1.519 \text{ g}\cdot\text{cm}^{-3}$, $\mu(\text{Mo-K}\alpha) = 13.89 \text{ cm}^{-1}$, $F(000) = 2352$, 11275 reflections in $h(-12/12)$, $k(-28/28)$, $l(-28/28)$, measured in the range $1.84^\circ \leq \theta \leq 27.49^\circ$, completeness $\theta_{\text{max}} = 99.7\%$, 11275 independent reflections, 9902 reflections with $F_o > 4(F_\sigma)$, 591 parameters, $R1_{\text{obs}} = 0.045$, $wR2_{\text{obs}} = 0.106$, $R1_{\text{all}} = 0.057$, $wR2_{\text{all}} = 0.113$, GOOF = 1.047, Flack-parameter 0.08(1), largest difference peak and hole: $0.652/-0.534 \text{ e}\cdot\text{\AA}^{-3}$.

Solid State NMR Spectroscopy: The ^{13}C solid state NMR spectra were measured with three different solid state NMR spectrometers, namely a Bruker AMX 400, a Varian Unity 500, and a Varian CMX Infinity 600 plus at fields of 9.4, 11.7, and 14 T, respectively. All spectra were recorded under high power proton decoupling at ambient temperature. The spectra of **1**, **2**, and **1a** were measured employing a variable amplitude cross polarization with a contact time of 1.2 ms. For the insertion product **2a** we were not able to obtain a signal from the suspected thiocarbonyl group with this technique. We therefore did additional measurements employing ^{13}C 90° pulse excitation on this sample, using a recycle time of 100 s. In this experiment, we were able to reveal the thiocarbonyl signal (see Supporting Information). While the spectral assignment of the thiocarbonyl groups is obvious from the prominent chemical shift, the assignment of the aromatic and aliphatic carbons was done employing simulations with the NMR predictor program of ACDlabs.

Reactions of 1a

Methyl Iodide: CS_2 (300 μL , 5 mmol) was added to a solution of **1a** (251 mg, 0.5 mmol) in chloroform (1 mL). After 30 min. methyl iodide (310 μL , 5 mmol) was added and the mixture was stirred overnight. The solvents were removed and the residue was washed several times with pentane. The combined pentane extracts were concentrated and chromatographed on 20 cm^3 of silica (eluent: pentane). After the elution of benzyl methyl sulfide (12 mg, 0.087 mmol), which was collected separately, benzyl methyl trithiocarbonate (**3**) (82 mg, 0.38 mmol, 76%) was obtained as a yellow oil. The substance was identified by NMR analyses and compared with data from the literature.^[26] ^1H NMR (250 MHz, CDCl_3): $\delta = 2.78$ (s, 3 H, CH_3), 4.66 (s, 2 H, CH_2), 7.26–7.41 (m, 5 H, C_6H_5) ppm. ^{13}C NMR (62.5 MHz, CDCl_3): $\delta = 20.2$, 41.6, 127.8, 128.7, 129.3, 135.1, 224.2 ppm.

Acetyl Chloride: CS_2 (300 μL , 5 mmol) was added to a solution of **1** (251 mg, 0.5 mmol) in chloroform (1 mL). After 30 min. acetyl chloride (36 μL , 0.5 mmol) was added while stirring. After 20 min the mixture was subjected to chromatography on 20 cm^3 of silica (eluent: CHCl_3). **4** (88 mg, 72%) was isolated and identified by ^1H and ^{13}C NMR spectra.

Synthesis of 4 (Reference Sample): Benzyl mercaptan (205 mg, 1.65 mmol) was added to a solution of KOH (92.7 mg, 1.65 mmol) in methanol (10 mL). After stirring for 30 min at room temp., the solvent was removed under reduced pressure. The residue was carefully dried in a desiccator. The salt was dissolved in dried THF (5 mL) and an excess of CS_2 (0.84 mL, 14 mmol) was added at 0°C . The temperature was raised to 25°C after stirring for 60 min. The reaction mixture was then cooled to -78°C . Acetyl chloride (0.178 mL, 2.5 mmol) was added dropwise, whereupon the yellow solution turned red. After stirring for 20 min the solvent was evaporated. The residue was purified by chromatography on silica (eluent: CHCl_3), yielding 107 mg (27%) of a red oil that decomposed at room temp. within a few weeks. $\text{C}_6\text{H}_5\text{-CH}_2\text{-S-C(S)-S-C(O)-CH}_3$ ($\text{C}_{10}\text{H}_{10}\text{OS}_3$) (242.39): calcd. C 49.55, H 4.16, S 39.20; found C 50.28, H 4.10, S 39.20. ^1H NMR (250 MHz, CDCl_3): $\delta = 2.41$ (s, 3 H, CH_3), 4.49 (s, 2 H, CH_2), 7.28–7.36 (m, 5 H, C_6H_5) ppm. ^{13}C NMR (62.5 MHz, CDCl_3): $\delta = 29.8$, 42.9, 128.0, 128.8, 129.4, 133.8, 189.9, 212.4 ppm.

Kinetics

Experimental Setup: The insertion of CS_2 was monitored by UV/Vis spectroscopy. Complex **1a** shows an absorption maximum at 434 nm, whereas the starting complex **1** does not show any absorption in the visible range at all. Measurements were performed using a Cary 5000 UV/Vis spectrometer from Varian. For keeping the temperature constant, a Cary dual cell peltier accessory from Varian was used. 1 cm quartz cuvettes were obtained from Hellma. During the reaction the mixture was stirred with a magnetic stirrer. The reaction temperature was determined with a sensor that was placed directly in the reaction medium.

Measurements: An amount of 2 mL was placed into a cuvette from a 20 mM stock solution (502.4 mg of **1** in 50 mL of chloroform). After the desired temperature was reached, 48 μL (61 mg, 800 μmol) of CS_2 was added and data collection was started. For the first 60 s, data were collected every second and later every 10 s. The reactions were monitored until no further alteration of the absorbance could be detected. For details on the data analysis see Supporting Information.

Computational Details

Full geometry optimizations, i.e. without constraints, as well as frequency calculations on the stationary points thus obtained were carried out using the Gaussian03^[27] program package. Depending on the number of imaginary modes all points on the hypersurface were rigorously characterized as true minima (no imaginary mode) or transition structures (exactly one).

All optimizations were performed using the hybrid B3LYP^[28] density functional method, which includes the use of a term that accounts for the effect of dynamic electron correlation (Coulomb hole).^[29] Geometries were optimized in the gas phase using the standard 6-311+G(d) basis set.

To estimate solvent effects, single point calculations in the presence of a dielectric field, as described by the C-PCM model,^[30–32] were carried out on the gas phase geometries. In this model, the species of interest are embedded in a cavity of molecular shape surrounded by a polarizable continuum whose field is described by polarization

charges distributed on the cavity surface. This procedure is known to be very good at reproducing experimental hydration energies.^[30] In the framework of the C-PCM model the default UA0 cavities (based on the united atom topological model) and the dielectric constant of chloroform ($\epsilon = 4.9$) were used.

For all single point calculations the B98^[33] functional was used. The G3MP2Large basis set^[34] was employed on all atoms except zinc where the 6-311+G(3df) basis set as implemented in Gaussian03 was applied. The B98 density functional was chosen for the calculation of the energies because it has recently been shown that it outperforms the more popular B3LYP functional, both for absolute energies and barrier heights, especially for larger molecules.^[35–37] In all these studies the assessment was performed using single point calculations on some reference geometry, basically the same approach that we used in this work. We therefore believe that the use of the well-established B3LYP density functional for the geometry optimizations has only a minor effect on the calculated energies. This is even more plausible with respect to the fact that geometry relaxation effects from the dielectric field of the solvent are completely neglected. The absolute error of B98 on the G3/05 set is approximately $14 \text{ kJ}\cdot\text{mol}^{-1}$,^[35] but the relative errors are generally smaller.

All energies were calculated by adding the appropriate thermodynamic corrections [gas phase, B3LYP/6-311+G(d)] to the total free energy in solution (including electrostatic and nonelectrostatic terms) obtained from the single point calculations (B98/G3MP2Large). The gas phase correction values were calculated with the standard thermodynamic routines in Gaussian03 (with $T = 298.15 \text{ K}$ and $p = 1 \text{ atm}$) using the frequencies computed at the B3LYP/6-311+G(d) optimal gas phase geometries.

Supporting Information (see footnote on the first page of this article): Details are given on the Raman spectroscopy (including two spectra), the solid-state NMR spectroscopy (including four spectra), and the analysis of the kinetic data (including two kinetic plots). The Cartesian coordinates and absolute energies of all calculated structures are provided.

Acknowledgments

Financial support of this work by the Deutsche Forschungsgemeinschaft, SFB 436 “Metal Mediated Reactions Modeled After Nature” is gratefully acknowledged.

- [1] J. Notni, H. Görls, E. Anders, *Eur. J. Inorg. Chem.* **2006**, 1444–1455.
- [2] G. Parkin, *Chem. Rev. (Washington, DC, U. S.)* **2004**, *104*, 699–767.
- [3] F. Botre, G. Gros, B. T. Storey, *Carbonic Anhydrase*, VCH, New York, **1991**.
- [4] I. Bertini, C. Luchinat, W. Maret, M. Zeppezauer, *Zinc Enzymes*, Birkhäuser, Boston, **1986**.
- [5] S. Schenk, J. Kesselmeier, E. Anders, *Chem. Eur. J.* **2004**, *10*, 3091–3105.
- [6] M. Mauksch, M. Bräuer, J. Weston, E. Anders, *ChemBioChem* **2001**, *2*, 190–198.
- [7] M. Bräuer, J. L. Pérez-Lustres, J. Weston, E. Anders, *Inorg. Chem.* **2002**, *41*, 1454–1463.
- [8] U. Kuhn, C. Ammann, A. Wolf, F. X. Meixner, M. O. Andreae, J. Kesselmeier, *Atmos. Environ.* **1999**, *33*, 995–1008.
- [9] G. Protoschill-Krebs, C. Wilhelm, J. Kesselmeier, *Atmos. Environ.* **1996**, *30*, 3151–3156.
- [10] S. Blezinger, C. Wilhelm, J. Kesselmeier, *Biogeochemistry* **2000**, *48*, 185–197.
- [11] U. Kuhn, A. Wolf, C. Gries, T. H. Nash, J. Kesselmeier, *Atmos. Environ.* **2000**, *34*, 4867–4878.
- [12] J. Kesselmeier, A. Hubert, *Atmos. Environ.* **2002**, *36*, 4679–4686.
- [13] M. Bräuer, E. Anders, S. Sinnecker, W. Koch, M. Rombach, H. Brombacher, H. Vahrenkamp, *Chem. Commun.* **2000**, 647–648.
- [14] S. Sinnecker, M. Bräuer, W. Koch, E. Anders, *Inorg. Chem.* **2001**, *40*, 1006–1013.
- [15] M. Rombach, H. Vahrenkamp, *Inorg. Chem.* **2001**, *40*, 6144–6150.
- [16] R. Luckay, T. E. Chantson, J. H. Reibenspies, R. D. Hancock, *J. Chem. Soc., Dalton Trans.* **1995**, 1363–1367.
- [17] F. Wagner, M. T. Mocella, M. J. D’Aniello Jr, A. H.-J. Wang, E. K. Barefield, *J. Am. Chem. Soc.* **1974**, *96*, 2625–2627.
- [18] D. Schröder, H. Schwarz, S. Schenk, E. Anders, *Angew. Chem. Int. Ed.* **2003**, *42*, 5087–5090; *Angew. Chem.* **2003**, *115*, 5241–5244.
- [19] A. Bottoni, C. Z. Lanza, G. P. Miscione, D. Spinelli, *J. Am. Chem. Soc.* **2004**, *126*, 1542–1550.
- [20] *Molen, an interactive structure solution procedure*, 1999, Enraf-Nonius, Delft, The Netherlands.
- [21] *Collect, data collection software*, 1998, Nonius, The Netherlands.
- [22] G. M. Sheldrick, *Acta Crystallogr., Sect. A: Found. Crystallogr.* **1990**, *46*, 467–473.
- [23] G. M. Sheldrick, *Shelxl-97, release 97-2*, 1997, University of Göttingen, Germany, <http://shelx.uni-ac.gwdg.de/SHELXL/>.
- [24] A. L. Spek, *Platon, a multipurpose crystallographic tool*, 2004, Utrecht University, Utrecht, The Netherlands, <http://www.cryst.chem.uu.nl/platon>.
- [25] CCDC-258933 (for **1a**) and -286778 (for **2a**) contain the supplementary crystallographic data for this paper. These data can be obtained free of charge from The Cambridge Crystallographic Data Centre via http://www.ccdc.cam.ac.uk/data_request/cif.
- [26] S. Tanimoto, T. Oida, H. Ikehira, M. Okano, *Bull. Chem. Soc. Jpn.* **1982**, *55*, 1977–1978.
- [27] M. J. Frisch, G. W. Trucks, H. B. Schlegel, G. E. Scuseria, M. A. Robb, J. R. Cheeseman, J. A. J. A. Montgomery Jr, T. Vreven, K. N. Kudin, J. C. Burant, J. M. Millam, S. S. Iyengar, J. Tomasi, V. Barone, B. Mennucci, M. Cossi, G. Scalmani, N. Rega, G. A. Petersson, H. Nakatsuji, M. Hada, M. Ehara, K. Toyota, R. Fukuda, J. Hasegawa, M. Ishida, T. Nakajima, Y. Honda, O. Kitao, H. Nakai, M. Klene, X. Li, J. E. Knox, H. P. Hratchian, J. B. Cross, C. Adamo, J. Jaramillo, R. Gomperts, R. E. Stratmann, O. Yazyev, A. J. Austin, R. Cammi, C. Pomelli, J. W. Ochterski, P. Y. Ayala, K. Morokuma, G. A. Voth, P. Salvador, J. J. Dannenberg, V. G. Zakrzewski, S. Dapprich, A. D. Daniels, M. C. Strain, O. Farkas, D. K. Malick, A. D. Rabuck, K. Raghavachari, J. B. Foresman, J. V. Ortiz, Q. Cui, A. G. Baboul, S. Clifford, J. Cioslowski, B. B. Stefanov, G. Liu, A. Liashenko, P. Piskorz, I. Komaromi, R. L. Martin, D. J. Fox, T. Keith, M. A. Al-Laham, C. Y. Peng, A. Nanayakkara, M. Challacombe, P. M. W. Gill, B. Johnson, W. Chen, M. W. Wong, C. Gonzalez, J. A. Pople, *Gaussian03, revision C.02*, 2004, Gaussian, Inc., Wallingford, CT, <http://www.gaussian.com>.
- [28] A. D. Becke, *J. Chem. Phys.* **1993**, *98*, 5648–5652.
- [29] C. Lee, W. Yang, R. G. Parr, *Phys. Rev. B: Condens. Matter Mater. Phys.* **1988**, *37*, 785–789.
- [30] V. Barone, M. Cossi, *J. Phys. Chem. A* **1998**, *102*, 1995–2001.
- [31] M. Cossi, N. Rega, G. Scalmani, V. Barone, *J. Comput. Chem.* **2003**, *24*, 669–681.
- [32] A. Klamt, G. Schüürmann, *J. Chem. Soc., Perkin Trans. 2* **1993**, 799–805.
- [33] H. L. Schmider, A. D. Becke, *J. Chem. Phys.* **1998**, *108*, 9624–9631.

- [34] L. A. Curtiss, P. C. Redfern, K. Raghavachari, V. Rassolov, J. A. Pople, *J. Chem. Phys.* **1999**, *110*, 4703–4709.
- [35] L. A. Curtiss, P. C. Redfern, K. Raghavachari, *J. Chem. Phys.* **2005**, *123*, 124107–124119.
- [36] S. Andersson, M. Grüning, *J. Phys. Chem. A* **2004**, *108*, 7621–7636.
- [37] Y. Zhao, J. Pu, B. J. Lynch, D. G. Truhlar, *Phys. Chem. Chem. Phys.* **2004**, *6*, 673–676.

Received: October 26, 2005
Published Online: May 3, 2006